^{1}H NMR in Solution and Solid State Structural Study of Lanthanide(III) Cryptates

C. Platas,[†] F. Avecilla,[†] A. de Blas,[†] C. F. G. C. Geraldes,*[,‡] T. Rodríguez-Blas,*[,†] H. Adams,[§] and J. Mahía[||]

Departamento de Química Fundamental e Industrial, Universidade da Coruña, Campus de A. Zapateira, s/n 15071 A Coruña, Spain, Departamento de Bioquímica, Faculdade de Ciências e Tecnologia da Universidade de Coimbra, Apartado 3126, 3000 Coimbra, Portugal, Department of Chemistry, The University, Sheffield S3 7HF, UK, and Servicios Xerais de Apoio á Investigación, Universidade da Coruña, Spain

Received November 13, 1998

We present here a detailed structural comparison, both in the solid state and in aqueous solution, of a complete series of lanthanide cryptate complexes of a Schiff base axial macrobicyclic ligand L of general formula [LnL]-$[NO_3]_3 \cdot xH_2O$ (Ln = La−Lu, Y); the macrobicyclic receptor L is an azacryptand $N[(CH_2)_2N{=}CH{-}R{-}CH{=}N{-}(CH_2)_2]_3N$ (R = *m*-C_6H_2OH-2-Me-5). The crystal structures of the Ce, Nd, and Eu complexes, chemical formulae $[CeL(NO_3)](NO_3)_2 \cdot 1.5H_2O \cdot 0.5CH_3CH_2OH$ (**3**), $[NdL(NO_3)](NO_3)_2 \cdot 3H_2O$ (**5**), and $[EuL(NO_3)](NO_3)_2 \cdot H_2O \cdot CH_3OH$ (**7**), as well as that of $[YL(NO_3)][Y(NO_3)_3(H_2O)_2EtOH](NO_3)_2.EtOH \cdot CH_3CN$ (**16**), have been determined by single-crystal X-ray crystallography. The four crystals crystallize in the triclinic space group $P\bar{1}$ with $Z = 2$; $a = 10.853(3)$ Å, $b = 12.746(3)$ Å, $c = 17.907(5)$ Å, $\alpha = 98.09(2)°$, $\beta = 89.99(2)°$, $\gamma = 96.34(2)°$, for **3**; $a = 10.835(2)$ Å, $b = 12.544(3)$ Å, $c = 17.701(2)$ Å, $\alpha = 82.220(10)°$, $\beta = 89.240(10)°$, $\gamma = 84.45(2)°$ for **5**; $a = 10.896(2)$ Å, $b = 12.566(4)$ Å, $c = 17.688(3)$ Å, $\alpha = 81.23(2)°$, $\beta = 89.500(10)°$, $\gamma = 84.72(3)°$ for **7**; and $a = 12.723(2)$ Å, $b = 14.047(3)$ Å, $c = 16.943(2)$ Å, $\alpha = 66.07(2)°$, $\beta = 79.838(12)°$, $\gamma = 81.616(14)°$ for **16**. In light of their crystal structures, it can be stated that all of them adopt very similar structures, with the nine-coordinated metal ion bound asymmetrically to seven donor atoms in the ligand cavity and also to two oxygen atoms of a bidentate nitrate anion. The macrobicycle cavity adapts to the lanthanide contraction, while preserving the pseudo-triple-helix conformation around the metal ion. The coordination geometry of the metal atom is best considered as a slightly distorted monocapped dodecahedron. The aqueous solution structures of the paramagnetic complexes were thoroughly characterized from the proton NMR LIS and LIR data, with particular attention to the changes induced by the lanthanide contraction, and agree quite well with the crystal structures of the Nd and Y complexes. The experimental Ln−donor distances decrease progressively along the lanthanide series both in the solid and solution structures, but no drastic structural changes occur. The gradual contraction and distortion of the coordination polyhedron along the series cause a variation of the crystal field parameter $A_2^\circ\langle r^2\rangle$ and the hyperfine constants A_i of the lanthanides in the middle of the series, leading to "breaks" in the contact−pseudo-contact shift separation plots of the proton LIS values. However, this affects only slightly the geometric terms G_i of the protons and not at all their R_{ik} ratios. The conformational rigidity of the five-membered chelate rings formed by the metal-bound ethylenediamino moieties of the bound cryptand increases upon lanthanide contraction. The $\Delta G^\ddagger$ value for the $\delta \leftrightarrow \lambda$ conformational interconversion process of those rings is 70 ± 3 kJ for the Y complex.

Introduction

Lanthanide(III) complexes with encapsulating ligands have been the subject of numerous studies in recent years due to their potential applications in selective extraction of metals, NMR imaging contrast agents, fluoroimmunoassay, and diagnostic agents.[1]

Macrocyclic compartmental ligands have been systematically investigated for the preparation of mono- and polynuclear lanthanide complexes,[2] but improved protection of the Ln(III) ions from the solvent is expected to be obtained with macrobicyclic ligands; in fact, it has been stated that this type of ligands could enhance some interesting properties that make their lanthanide-(III) complexes valuable for the development of technological applications.[3] Many metal complexes with cryptands derived from the condensation of tris(2-aminoethyl)amine and 2,6-diformylphenols have been reported in the literature in the recent past. These Schiff-base axial macrobicyclic[4] ligands have been shown to form stable complexes with a wide range of metal ions,[5] including mononuclear[6−8] and binuclear[9] Ln(III) complexes.

The utility of paramagnetic lanthanide (III) complexes as an aid in determining molecular structure and conformation in

* To whom correspondence should be addressed. Tel.: +351 39 824531. Fax: +351 39 853607. E-mail: geraldes@cygnus.ci.uc.pt.
† DCFI, Universidade de Coruña.
‡ Universidade de Coimbra.
§ University of Sheffield.
|| SXAI, Universidade de Coruña.

(1) Alexander, V. *Chem. Rev.* **1995**, *95*, 273.
(2) Guerriero, P.; Tamburini S.; Vigato P. A. *Coord. Chem. Rev.* **1995**, *139*, 17.
(3) Sabbatini, N.; Guardigli, M.; Lehn, J. M. *Coord. Chem. Rev.* **1993**, *123*, 201.
(4) The term *axial macrobicycle* describes symmetrical molecules with coaxial arrangement of two tripodal subunits linked by three identical bridges. See: Lehn, J.-M. *Pure Appl. Chem.* **1980**, *52*, 2441.

10.1021/ic981314e CCC: $18.00
Published on Web 06/05/1999

Chart 1

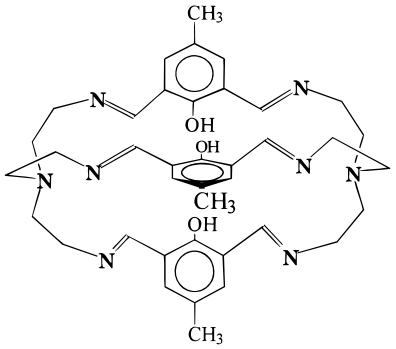

solution is well established.[10,11] Using the NMR spectral data of paramagnetic compounds, the separation of the contact and pseudo-contact contributions to the observed lanthanide induced shifts (LIS) can be accomplished. These pseudo-contact LIS values and the observed lanthanide induced relaxation (LIR) effects can be used to obtain the structure and dynamics in solution.[10] Although the solution structure of several diamagnetic and paramagnetic lanthanide(III) complexes of triaza or tetraaza macrocyclic ligands bearing pendant arms[12] and texaphyrins[13] have been studied by NMR spectroscopy and X-ray single-crystal data have been used to assess the agreement between the solid state and NMR solution structures,[13] up to now no such studies have been reported for lanthanide(III) complexes with cryptands. Herein we compare the structure in the solid state and in aqueous solution of the series of complexes $[LnL][NO_3]_3 \cdot xH_2O$ (Ln = La − Lu, Y) where L is the axial macrobicycle derived from the 2+3 condensation of tren and 2,6-diformyl-4-methylphenol (see Chart 1).

Experimental Section

Measurements. Elemental analyses were carried out on a Carlo Erba EA 1108 elemental analyzer. The IR spectra were recorded, as KBr disks, using a Perkin-Elmer 1330 spectrometer, and FAB mass spectra were recorded using a Fisons Quattro mass spectrometer with a cesium-ion gun and thioglycerol as matrix. High-resolution ^{1}H NMR spectra were recorded in D_2O solutions on Nicolet NT-200WB and Varian Unity-500 NMR spectrometers operating at 200.015 and 499.824 MHz, respectively. 3-(Trimethylsilyl)-1-propanesulfonic acid (deuterated, sodium salt) was used as internal chemical shift reference. Temperature calibration was checked using ethylene glycol and methanol samples. Longitudinal ^{1}H relaxation times (T_1) were measured by the inversion−recovery pulse sequence. Transverse relaxation times (T_2) were measured from the width of the peaks at half-height. The paramagnetic contributions to the relaxation rates were corrected for diamagnetic effects using the T_1 values and the line widths for the La complex under the same experimental conditions. ^{1}H NMR spectra of the diamagnetic complexes (La, Lu, Y) were assigned using two-dimensional (1024 × 2048 data points in F1 and F2) COSY and NOESY (0.5 or 0.8 s mixing time) experiments. The ^{1}H NMR spectra of the paramagnetic complexes were assigned by comparison of the experimental and calculated LIS and LIR values (see later).

Conductivity measurements were carried out in ca. 10^{-3} mol dm^{-3} dimethylformamide solutions at 20 °C using a Crison Micro CM 2201 conductivimeter.

Analysis of LIS and LIR Data. The LIS and LIR data were analyzed with the aid of the computer program LISLIR,[14] which allows us to vary the location of the lanthanide ion and of the main magnetic axis in a structure defined by its Cartesian coordinates and calculates the pseudo-contact LIS (assuming axial symmetry) and LIR values for each geometry. The calculated LIS and LIR values of pseudo-symmetry-related nuclei in the structure are averaged before comparison to experimental values. The constants $A_2^{\circ}\langle r^2\rangle$ (in eq 1) and k (in eq 5) are used as scaling factors between observed and calculated LIS and LIR values. The best fit between the experimental and calculated proton data is obtained with the aid of the LISLIR program, which performs a linear least-squares search and minimizes the difference between calculated and observed LIS and LIR data. The agreement between the observed and the calculated values is evaluated using Hamilton's crystallographic agreement factor (R factor)[15] defined as $R = ([\Sigma_i(f_{oi} - f_{ci})^2 w_i]/(\Sigma_i f_{oi}))^{1/2}$, where f_{oi} and f_{ci} are observed and calculated values, respectively, and w_i are weighting factors.

Materials. 2,6-Diformyl-4-methylphenol was prepared according to the literature method.[16] Tris(2-aminoethyl)amine and the lanthanide(III) nitrates were from Aldrich and Alfa Laboratories, used without further purification. Solvents were of reagent grade purified by the usual methods. Deuterated solvents for NMR (D_2O, NaOD, DCl) were obtained from Sigma.

Preparation of the Complexes. $[YL(NO_3)](NO_3)_2 \cdot 3H_2O$ (1). To a stirred solution of the $Y(NO_3)_3 \cdot 5H_2O$ (0.91 g; 0.25 mmol) and 2,6-diformyl-4-methylphenol (0.123 g; 0.75 mmol) in hot absolute ethanol (40 mL) was added dropwise a solution of tris(2-aminoethyl)amine (0.075 mL; 0.5 mmol) also in absolute ethanol (30 mL). The solution became turbid during the addition, and a yellow precipitate appeared. After the addition was completed, the resulting yellow solution was stirred and heated to reflux for 12 h. The precipitate was removed by filtration, and the filtrate was concentrated to 20 mL under vacuum. The yellow precipitate formed was filtered off, and the filtrate was left to evaporate slowly at room temperature to yield a yellow microcrystalline powder. The complex was isolated by filtration and was washed with diethyl ether and dried under vacuum over $CaCl_2$. Yield: 0.075 g (30%). Anal. Calcd for $C_{39}H_{54}N_{11}O_{15}Y$: C, 46.6; H, 5.4; N, 15.3. Found: C, 46.9; H, 5.2; N, 15.0. Λ_m (Ω^{-1} cm^2 mol^{-1}): 142. MS−FAB (m/z): 763 [**1** − 2H − $3NO_3$], 826 [**1** − H − $2NO_3$]. IR (fluorolube): 1651 cm^{-1}.

$[LaL(NO_3)](NO_3)_2 \cdot 4H_2O$ (2). The yellow complex was prepared as described for **1** by using $La(NO_3)_3 \cdot 6H_2O$ (0.108 g; 0.25 mmol). Yield: 0.115 g (43%). Anal. Calcd for $C_{39}H_{56}LaN_{11}O_{16}$: C, 43.6; H,

(5) Nelson, J.; McKee, V.; Morgan, G. *Prog. Inorg. Chem.* **1998**, *47*, 167.
(6) Drew, M. G. B.; Howarth, O. W.; Harding, C. J.; Martin, N.; Nelson, J. *J. Chem. Soc., Chem. Commun.* **1995**, 903.
(7) (a) Hu, S.-Y.; Huang, Q.; Wu, B.; Zhang, W.-J.; Wu, X.-T. *J. Chem. Soc., Dalton Trans.* **1996**, 3883.(b) Yu, S.-Y.; Wang, Q.-M.; Wu, B.; Wu, X.-T.; Hu, H.-M.; Wang, L.-F.; Wu, A.-X. *Polyhedron* **1997**, *16*, 321. (c) Feng, C.-J.; Luo, Q.-H.; Duan, C.-Y.; Shen, M.-C.; Lau, Y.-J. *J. Chem. Soc., Dalton Trans.* **1998**, 1377.
(8) Avecilla, F.; Bastida, R.; de Blas, A.; Fenton, D. E.; Macías, A.; Rodríguez, A. Rodríguez-Blas, T.; García-Granda, S.; Corzo-Suárez, R. *J. Chem. Soc., Dalton Trans.* **1997**, 409.
(9) Avecilla, F.; De Blas, A.; Bastida, R.; Fenton D. E.; Mahía, J.; Macías, A.; Rodríguez A.; Rodríguez-Blas, T. *J. Chem. Soc., Chem. Commun.* **1999**, 125.
(10) Sherry, A. D.; Geraldes, C. F. G. C. *Lanthanide Probes in Life, Chemical and Earth Sciences*; Bünzli, J.-C. G., Choppin, G. R., Eds.; Elsevier: Amsterdam, 1989.
(11) Forsberg, J. H.; Delaney, R. M.; Zhao, Q.; Harakas, G.; Chandran, R. *Inorg. Chem.* **1995**, *34*, 3705.
(12) (a) Bryden, C. C.; Reilley, C. N.; Desreux, J. F. *Anal. Chem.* **1981**, *53*, 1418. (b) Desreux, J. F. *Inorg. Chem.* **1980**, *19*, 1319. (c) Geraldes, C. F. G. C.; Alpoim, M. C.; Marques, M. P. M.; Sherry, A. D.; Singh, M. *Inorg. Chem.* **1985**, *24*, 3876. (d) Sherry, A. D.; Singh, M.; Geraldes, C. F. G. C. *J. Magn. Reson.* **1986**, *66*, 511. (e) Ascenso, J. R.; Delgado, R.; Frausto da Silva, J. J. R. *J. Chem. Soc., Dalton Trans.* **1986**, 2395. (f) Geraldes, C. F. G. C.; Sherry, A. D.; Kiefer, G. E. *J. Magn. Reson.* **1992**, *97*, 290. (g) Aime, S.; Botta, M.; Ermondi, G. *Inorg. Chem.* **1992**, *31*, 4291. (h) Chin, K. O. A.; Morrow, J. R.; Lake, C. H.; Churchill, M. R. *Inorg. Chem.* **1994**, *33*, 656. (i) Brittain, H. G.; Desreux, J. F. *Inorg. Chem.* **1984**, *23*, 4459.
(13) Lisowski, J.; Sessler, J. L.; Lynch, V.; Mody, T. D. *J. Am. Chem. Soc.* **1995**, *117*, 2273.
(14) (a) Peters, J. A.; Peters- van Cranenburgh, P. E. J.; van der Toorn, J. M.; Wortel, T. M.; van Bekkum, H. *Tetrahedron* **1978**, *34*, 2217. (b) Carvalho, R. A.; Peters, J. A.; Geraldes, C. F. G. C. *Inorg Chim. Acta* **1997**, *262*, 167.
(15) (a) Willcott, M. R.; Lenkinski, R. E.; Davis, R. E. *J. Am. Chem. Soc.* **1972**, *94*, 1742. (b) Davis, R. E.; Willcott, M. R. *J. Am. Chem. Soc.* **1972**, *94*, 1744.
(16) Taniguchi, S. *Bull. Chem. Soc. Jpn.* **1984**, *57*, 2683.

5.3; N, 14.3. Found: C, 43.3; H, 4.7; N, 13.9. Λ_m (Ω^{-1} cm^2 mol^{-1}): 145. MS−FAB (*m*/*z*): 813 [**2** − 2H − 3NO$_3$]. IR (fluorolube): 1651 cm^{-1}.

[CeL(NO$_3$)](NO$_3$)$_2$·H$_2$O (3). The yellow complex was prepared as described for **1** by using Ce(NO$_3$)$_3$·6H$_2$O (0.109 g; 0.25 mmol). Yield: 0.091 g (35%). Anal. Calcd for $CeC_{39}H_{50}N_{11}O_{13}$: C, 45.9; H, 4.9; N, 15.1. Found: C, 45.8; H, 5.3; N, 15.1. Λ_m (Ω^{-1} cm^2 mol^{-1}): 127. MS−FAB (*m*/*z*): 814 [**3** − 2H − 3NO$_3$]. IR (fluorolube): 1649 cm^{-1}. Orange crystals of formula [CeL(NO$_3$)](NO$_3$)$_2$·1.5H$_2$O·0.5CH$_3$CH$_2$OH suitable for X-ray diffraction were grown by slow evaporation of the mother liquor at room temperature.

[PrL(NO$_3$)](NO$_3$)$_2$·H$_2$O (4). The yellow complex was prepared as described for **1** by using Pr(NO$_3$)$_3$·6H$_2$O (0.109 g; 0.25 mmol). Yield: 0.088 g (34%). Anal. Calcd for $C_{39}H_{50}N_{11}PrO_{13}$: C, 45.8; H, 4.9; N, 15.1. Found: C, 45.8; H, 4.9; N, 14.7. Λ_m (Ω^{-1} cm^2 mol^{-1}): 142. MS−FAB (*m*/*z*): 815 [**4** − 2H − 3NO$_3$]. IR (fluorolube): 1649 cm^{-1}.

[NdL(NO$_3$)](NO$_3$)$_2$·4H$_2$O (5). The yellow complex was prepared as described for **1** by using Nd(NO$_3$)$_3$·6H$_2$O (0.110 g; 0.25 mmol). Yield: 0.062 g (23%). Anal. Calcd for $C_{39}H_{56}NdN_{11}O_{16}$: C, 43.4; H, 5.2; N, 14.3. Found: C, 43.7; H, 4.9; N, 14.0. Λ_m (Ω^{-1} cm^2 mol^{-1}): 149. MS−FAB (*m*/*z*): 818 [**5** − 2H − 3NO$_3$]. IR (fluorolube): 1651 cm^{-1}.

Crystals of formula [NdL(NO$_3$)](NO$_3$)$_2$·3H$_2$O suitable for X-ray diffraction were grown from an acetonitrile/toluene 1:1 solution of the isolated solid.

[SmL(NO$_3$)](NO$_3$)$_2$·H$_2$O (6). The yellow complex was prepared as described for **1** by using Sm(NO$_3$)$_3$·6H$_2$O (0.107 g; 0.25 mmol). Yield: 0.094 g (37%). Anal. Calcd. for $C_{39}H_{50}N_{11}O_{13}Sm$: C, 45.4; H, 5.0; N, 14.9. Found: C, 45.3; H, 4.9; N, 14.8. Λ_m (Ω^{-1} cm^2 mol^{-1}): 152. MS−FAB (*m*/*z*): 826 [**6** − 2H − 3NO$_3$], 889 [**6** − 2H − 2NO$_3$]. IR (fluorolube): 1651 cm^{-1}.

[EuL(NO$_3$)](NO$_3$)$_2$·4H$_2$O (7). The yellow complex was prepared as described for **1** by using Eu(NO$_3$)$_3$·6H$_2$O (0.112 g; 0.25 mmol. Yield: 0.066 g (29%). Anal. Calcd for $C_{39}H_{52}EuN_{11}O_{14}$: C, 44.6; H, 5.0; N, 14.7. Found: C, 44.8; H, 4.6; N, 14.3. Λ_m (Ω^{-1} cm^2 mol^{-1}): 127. MS−FAB (*m*/*z*): 827 [**7** − 2H − 3NO$_3$], 977 [**7** + Eu − 3H − 3NO$_3$], 1039 [**7** + Eu − 3H − 2NO$_3$], 1101 [**7** + Eu − 3H − NO$_3$]. IR (fluorolube): 1649 cm^{-1}. Crystals of formula [EuL(NO$_3$)](NO$_3$)$_2$·H$_2$O·CH$_3$OH suitable for X-ray diffraction were grown from an acetonitrile/toluene 1:1 solution of the isolated solid.

[GdL(NO$_3$)](NO$_3$)$_2$·H$_2$O (8). The yellow complex was prepared as described for **1** by using Gd(NO$_3$)$_3$·5H$_2$O (0.108 g; 0.25 mmol). Yield: 0.138 g (49%). Anal. Calcd for $C_{39}GdH_{50}N_{11}O_{13}$: C, 45.1; H, 4.8; N, 14.8. Found: C, 45.3; H, 4.7; N, 14.4. Λ_m (Ω^{-1} cm^2 mol^{-1}): 150. MS−FAB (*m*/*z*): 832 [**8** − 2H − 3NO$_3$]. IR (fluorolube): 1651 cm^{-1}.

[TbL(NO$_3$)](NO$_3$)$_2$·2H$_2$O (9). The yellow complex was prepared as described for **1** by using Tb(NO$_3$)$_3$·5H$_2$O (0.109 g; 0.25 mmol). Yield: 0.100 g (41%). Anal. Calcd for $C_{39}H_{52}N_{11}O_{14}Tb$: C, 44.3; H, 4.9; N, 14.6. Found: C, 44.6; H, 4.9; N, 14.6. Λ_m (Ω^{-1} cm^2 mol^{-1}): 134. MS−FAB (*m*/*z*): 833 [**9** − 2H − 3NO$_3$]. IR (fluorolube): 1651 cm^{-1}.

[DyL(NO$_3$)](NO$_3$)$_2$·H$_2$O (10). The yellow complex was prepared as described for **1** by using Dy(NO$_3$)$_3$·5H$_2$O (0.110 g; 0.25 mmol). Yield: 0.078 g (30%). Anal. Calcd for $C_{39}DyH_{50}N_{11}O_{13}$: C, 44.9; H, 4.8; N, 14.8. Found: C, 44.9; H, 5.1; N, 14.8. Λ_m (Ω^{-1} cm^2 mol^{-1}): 148. MS−FAB (*m*/*z*): 838 [**10** − 2H − 3NO$_3$]. IR (fluorolube): 1649 cm^{-1}.

[HoL(NO$_3$)](NO$_3$)$_2$·H$_2$O (11). The yellow complex was prepared as described for **1** by using Ho(NO$_3$)$_3$·5H$_2$O (0.110 g; 0.25 mmol). Yield: 0.154 g (57%). Anal. Calcd for $C_{39}H_{50}HoN_{11}O_{13}$: C, 44.8; H, 4.8; N, 14.7. Found: C, 44.7; H, 5.0; N, 14.7. Λ_m (Ω^{-1} cm^2 mol^{-1}): 146. MS−FAB (*m*/*z*): 839 [**11** − 2H − 3NO$_3$]. IR (fluorolube): 1649 cm^{-1}.

[ErL(NO$_3$)](NO$_3$)$_2$·2H$_2$O (12). The yellow complex was prepared as described for **1** by using Er(NO$_3$)$_3$·5H$_2$O (0.111 g; 0.25 mmol). Yield: 0.070 g (26%). Anal. Calcd for $C_{39}ErH_{52}N_{11}O_{14}$: C, 43.9; H, 4.9; N, 14.5. Found: C, 44.4; H, 4.9; N, 14.6. Λ_m (Ω^{-1} cm^2 mol^{-1}): 153. MS−FAB (*m*/*z*): 842 [**12** − 2H − 3NO$_3$]. IR (fluorolube): 1649 cm^{-1}.

[TmL(NO$_3$)](NO$_3$)$_2$·2H$_2$O (13). The yellow complex was prepared as described for **1** by using Tm(NO$_3$)$_3$·5H$_2$O (0.111 g; 0.25 mmol). Yield: 0.127 g (47%). Anal. Calcd for $C_{39}H_{52}N_{11}O_{14}Tm$: C, 43.9; H, 4.9; N, 14.4. Found: C, 44.2; H, 4.8; N, 14.5. Λ_m (Ω^{-1} cm^2 mol^{-1}): 161. MS−FAB (*m*/*z*): 843 [**13** − 2H − 3NO$_3$]. IR (fluorolube): 1651 cm^{-1}.

[YbL(NO$_3$)](NO$_3$)$_2$·2H$_2$O (14). The yellow complex was prepared as described for **1** by using Yb(NO$_3$)$_3$·6H$_2$O (0.117 g; 0.25 mmol). Yield: 0.080 g (30%). Anal. Calcd for $C_{39}H_{52}N_{11}O_{14}Yb$: C, 43.7; H, 4.9; N, 14.4. Found: C, 44.0; H, 4.9; N, 14.2. Λ_m (Ω^{-1} cm^2 mol^{-1}): 161. MS−FAB (*m*/*z*): 848 [**14** − 2H − 3NO$_3$]. IR (fluorolube): 1649 cm^{-1}.

[LuL(NO$_3$)](NO$_3$)$_2$·4H$_2$O (15). The yellow complex was prepared as described for **1** by using Lu(NO$_3$)$_3$·5H$_2$O (0.1113 g; 0.25 mmol). Yield: 0.062 g (23%). Anal. Calcd for $C_{39}H_{56}LuN_{11}O_{16}$: C, 42.2; H, 5.1; N, 13.9. Found: C, 42.2; H, 4.7; N, 13.7. Λ_m (Ω^{-1} cm^2 mol^{-1}): 147. MS−FAB (*m*/*z*): 849 [**15** − 2H − 3NO$_3$]. IR (fluorolube): 1649 cm^{-1}.

[YL(NO$_3$)][Y(NO$_3$)$_3$(H$_2$O)$_2$EtOH](NO$_3$)$_2$·EtOH·CH$_3$CN (16). The yellow complex was synthesized as described previously.[8] Crystals suitable for X-ray diffraction were grown from an acetonitrile/toluene 1:1 solution of the isolated solid.

Crystal Structure Determination of Complexes 3, 5, and 7. X-ray data were collected at room temperature in the range $3.5 < 2\theta < 45°$ on a Nicolet R3 diffractometer by the ω scan method. 7574 reflections were measured for **3** (dimensions 0.43 × 0.28 × 0.22 mm), 7772 for **5** (0.55 × 0.33 × 0.22 mm), and 7342 for **7** (0.55 × 0.33 × 0.22 mm), all of which were corrected for Lorentz and polarization effects (but not for absorption), 5406, 5594, and 5646 independent reflections exceeded, respectively, the significance level $|F|/\sigma(|F|) > 4.0$. The structure was solved by direct methods and refined by full-matrix least-squares methods on F^2. Hydrogen atoms were included in calculated positions and refined in riding mode. Hydrogen atoms for some solvent molecules were not included. For **3** convergence was reached at a final $R = 0.0521$, w$R_2 = 0.1429$, 581 parameters for all unique 6362 data with allowance for thermal anisotropy of all non-hydrogen atoms. Minimum and maximum final electron density: −0.665 and 1.487 e Å^{-3}. For **5** convergence was reached at a final $R = 0.0477$, wR_2 = 0.1400, 560 parameters for all unique 6199 data with allowance for thermal anisotropy of all non-hydrogen atoms. No residual density was found outside −0.715 and 1.373 e Å^{-3}. For **7** convergence was reached at $R = 0.0566$, w$R_2 = 0.1528$, 568 parameters for all unique 6215 data with allowance for thermal anisotropy of all non-hydrogen atoms. A final difference Fourier map showed no residual density outside −1.835 and 1.491 e Å^{-3}. In all cases, complex scattering factors were taken from the program package SHELXL93[17] as implemented on the Viglen 486dx computer. Crystal data and details on data collection and refinement are presented in Table 1.

Crystal Structure Determination for Complex 16. A yellow blocklike crystal of [Y$_2$C$_{39}$H$_{47}$N$_{14}$O$_{21}$]·2CH$_3$CH$_2$OH·CH$_3$CN·2H$_2$O (dimensions: 0.55 × 0.45 × 0.30 mm) was used for the structure determination. X-ray data were collected using a Siemens SMART CCD area detector single-crystal diffractometer. Preliminary unit cell constants were determined with a set of 45 narrow frames (0.3 in ω) scans. A total of 1255 frames of intensity data were collected with a frame width of 0.3 per frame in ω and counting time of 5 s/frame at a crystal to detector distance of 4.0 cm. A semiempirical absorption correction was carried out using an ellipsoidal model (maximum and minimum transmission coefficients, 0.533 and 0.314). The integration process yielded 11 546 reflections, of which 9102 were independent. The structure was solved using the Siemens SHELXTL-PC[18] software by direct methods and refined by full-matrix least-squares methods on F^2. Hydrogen atoms of the macrobicycle host (less those of the hydroxyl groups) were included in calculated positions and refined in riding

(17) Sheldrick, G. M. *SHELXL93: An Integrated System for Solving and Refining Crystal Structures from Diffraction Data*; University of Göttingen: Germany, 1997.

(18) Sheldrick, G. M. *SHELXTL: An Integrated System for Solving and Refining Crystal Structures from Diffraction Data*; University of Göttingen: Germany, 1997.

Table 1. Crystallographic Data for Complexes **3**, **5**, **7**, and **16**

	3	**5**	**7**	**16**
empirical formula	$C_{40}H_{54}N_{11}O_{14}Ce$	$C_{39}H_{54}N_{11}O_{15}Nd$	$C_{40}H_{54}N_{11}O_{14}Eu$	$C_{45}H_{45}N_{15}O_{25}Y_2$
fw	1053.06	1061.12	1064.90	1373.78
space group	$P\bar{1}$	$P\bar{1}$	$P\bar{1}$	$P\bar{1}$
cryst system	triclinic	triclinic	triclinic	triclinic
Z	2	2	2	2
a, Å	10.853(3)	10.835(2)	10.896(2)	12.723(2)
b, Å	12.746(3)	12.544(3)	12.566(4)	14.047(3)
c, Å	17.907(5)	17.701(2)	17.688(3)	16.943(3)
α, deg	98.09(2)	82.220(10)	81.23(2)	66.07(2)
β, deg	89.99(2)	89.240(10)	89.500(10)	79.838(12)
γ, deg	96.34(2)	84.45(2)	84.72(3)	81.616(14)
V, Å^3	2437.2(11)	2372.5(8)	2383.3(10)	2715.0(9)
ρ(calc), g/cm^3	1.435	1.477	1.484	1.680
μ_{calcd}, mm^{-1}	1.006	1.170	1.390	2.229
radiation (Mo Kα), Å	0.71073	0.71073	0.71073	0.71073
T, K	293(2)	293(2)	293(2)	133(2)
final R indices [$I > 2\sigma(I)$]	R1 = 0.0521; wR2 = 0.1429	R1 = 0.0477; wR2 = 0.1400	R1 = 0.0566; wR2 = 0.1528	R1 = 0.0890; wR2 = 0.2333
final R indices (for all data)	R1 = 0.0645; wR2 = 0.1511	R1 = 0.0536; wR2 = 0.1467	R1 = 0.0624; wR2 = 0.1587	R1 = 0.1184; wR2 = 0.2618

[a] $R1 = \sum||F_o| - |F_c||/\sum|F_o|$ and $wR2 = \{\sum[w(|F_o|^2 - |F_c|^2|)^2]/\sum[w(F_o^4)]\}^{1/2}$.

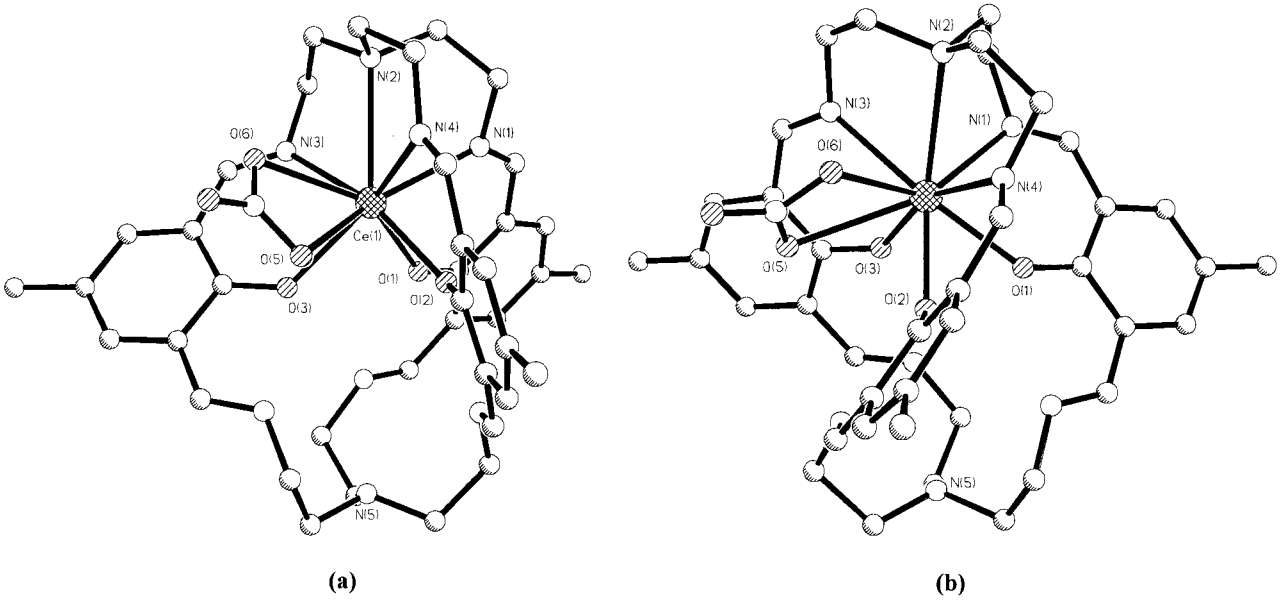

Figure 1. X-ray crystal structure of the cations $[LnL(NO_3)]^{2+}$ for (a) Ln = Ce (**3**) and (b) Ln = Nd, Eu (**5**, **7**) showing the atomic numbering scheme. Hydrogen atoms have been omitted for simplicity.

mode. Hydrogen atoms of solvent molecules were not included. Ionic nitrates and solvent molecules show high thermal parameters, so their geometries were constrained. The convergence was reached at a final $R = 0.0890$, $wR_2 = 0.2333$, 789 parameters for all unique 9097 data with allowance for thermal anisotropy of all non-hydrogen atoms. Minimum and maximum final electron density: −1.777 and 0.940 e Å^{-3}. A summary of the experimental and structural solution procedure is given in Table 1.

Results and Discussion

Synthesis and Characterization. The complexes of formula $LnL(NO_3)_3{\cdot}nH_2O$ (Ln = La − Lu except Pm and Y, $n = 1-4$) were prepared by a one-step procedure, as described in the Experimental Section, in moderate yields (23−57%). Crystals of the cerium complex, **3**, suitable for analysis by single-crystal X-ray diffraction were grown by slow evaporation of the mother liquor. Crystals of the neodymium (**5**) and europium (**7**) complexes suitable for X-ray diffraction were grown from an acetonitrile/toluene 1:1 solution of the isolated solid. The presence of an intense absorption band at ca.1650 cm^{-1} attributable to the $\nu(C{=}N)_{imine}$ stretching frequency in their infrared spectra (fluorolube mull) and the absence of bands due to the carbonyl and amine groups confirm that condensation and cyclization of the macrocycle has occurred. Further evidence for the formation of the macrobicycle and its complexation comes from the FAB mass spectra in which an intense peak corresponding to [Ln(L − 2H)]$^+$ appears in all cases.

Conductivity measurements were carried out at 10^{-3} M concentration in DMF solution. The molar conductance revealed that the complexes behave as 2:1 electrolytes in this solvent.[19]

X-ray Structures. Complexes 3, 5, and 7. Crystals of **3**, **5**, and **7** consist of the dications $[CeL(NO_3)]^{2+}$, $[NdL(NO_3)]^{2+}$, and $[EuL(NO_3)]^{2+}$, respectively, and two well-separated nitrate anions; crystal lattices also contain solvent and/or water molecules. Structures **5** and **7** are isomorphous, and Figure 1b illustrates the structure of both dications $[ML(NO_3)]^{2+}$ (M = Nd, Eu). **3** is not isomorphous with them and shows different

(19) Geary, W. J. *Coord. Chem. Rev.* **1971**, *7*, 81.

helicity in the strands as illustrated in Figure 1a; the crystal of **3** possesses different cell dimensions than those of **5** and **7** (Table 1).

In the three cation complexes, $[ML(NO_3)]^{2+}$, the metal ion is placed asymmetrically at one end of the cavity of the cryptand, and is nine coordinated, bound to three imino-nitrogen atoms, three phenolic oxygen atoms and one of the bridgehead nitrogen atoms. The distance between the lanthanide ion and the bridgehead nitrogen is considerably higher than those of the lanthanide ion and the imino-nitrogen atoms, showing a weak interaction between the amine nitrogen and the Ln(III) ion. A progressive decrease of the Ln-donor atom bond distances is observed upon decreasing the ionic radii of the lanthanide ions. The eighth and ninth positions are occupied by two oxygen atoms of a bidentate nitrate anion. The average distance between the metal ion and the coordinated nitrate oxygen atoms is 2.42 Å. Dimensions (distances and angles) of the metal coordination spheres are listed in Table 2. The atoms N(1), N(3), N(4), and O(6) form a plane with a deviation from planarity of 0.0993 Å in case of **3**, 0.1031 Å for **5**, and 0.0897 Å for **7**; the distance of the corresponding metal ion to this plane is 1.0429 Å (complex **3**), 1.0117 Å (**5**), and 0.9855 Å (**7**). It could be possible to describe the coordination polyhedron as a monocapped square antiprism in which the coordinated bridgehead nitrogen atom N(2) would be the cap, the four donors N(1), N(3), N(4), and O(6) would constitute the upper plane of the square antiprism and the other four donor atoms, O(1), O(2), O(3), and O(5), would form the basal plane; nevertheless, the deviation from planarity of this last plane (0.2020 Å in **3**, 0.1973 in **5**, and 0.2195 in **7**) is too large to consider that these four oxygen atoms are in a plane. We think that the coordination geometry of the metal ion is best considered as a slightly distorted monocapped dodecahedron where the O(5) of the coordinated nitrate group is the atom that is capping the dodecahedron.

With respect to the conformation that the macrobicycle L adopts in these three complexes, the nitrogen atoms of the C=N bonds are on the same side of the aromatic ring in the three chains, what is described as a *sss* conformation,[20] and not only the coordinated bridgehead nitrogen atom but also the other one that is not involved in the coordination of the metal ion are disposed in *endo* as shown in Figure 1. Likewise, the macrobicycle L is twisted around the axis that passes through both bridgehead nitrogen atoms resembling a triple helix. The angles between the planes defined by the phenolic rings are 66.6°, 84°, and 101.8° for **3**, 77.2°, 84.4°, and 112.5° for **5**, and 80.4°, 84.0°, and 111.6° for **7.** The distances between the bridgehead nitrogen atoms are 8.48, 8.46, and 8.46 Å for **3**, **5**, and **7**, respectively, and the distances between each two phenolic oxygen atoms are 2.825, 3.018, and 3.577 Å for **3**, 2.791, 2.965, and 3.490 Å for **5**, and 2.741, 2.924, and 3.378 Å for **7**.

Crystal Structure of 16. Crystals of **16** contain two different metal structural units, the cation $[YL(NO_3)]^{2+}$ and the neutral complex $[Y(NO_3)_3(H_2O)_2(EtOH)]$, two well-separated nitrate anions, a molecule of ethanol and a molecule of acetonitrile. Figure 2 illustrates the structure of both yttrium complexes and Table 2 summarizes selected bond lengths and angles. As shown in Figure 2a, in the neutral complex the yttrium ion is bound to nine oxygen atoms, six corresponding to three bidentate nitrate ions, two to two water molecules and one to an ethanol molecule. The coordination polyhedron may be described as a distorted tricapped trigonal prism in which O(1S), O(9), and O(14) form one of the triangular faces and the oxygen atoms, O(2S), O(3S), and O(10), form the other one; each oxygen atom, O(7), O(15), and O(11), is capping a quadrangular face. The distortion of the trigonal prism comes from the biplanar angle between both planes that has a value of 10.9°; likewise, both triangular faces are not fully eclipsed as expected in a regular trigonal prism.

In the cation complex (Figure 2b), there are two positions for the yttrium ion with occupancies of 0.95(1) and 0.05(1), respectively. The major position, Y(1), is found to one side of the cryptand, similar to **3**, **5**, and **7** previously described, where it is also bound to the three imino nitrogen atoms [2.476 (7), 2.532 (7), and 2.483 (6) Å], the three phenoxy oxygen atoms [2.382 (6), 2.245 (5), and 2.289 (5) Å] and a bridgehead nitrogen atom [2.695 (6) Å], and completes its coordination sphere with

Table 2. Dimensions (distances in Å, Angles in deg) of the Metal Coordination Spheres in Complexes **3**, **5**, **7**, and **16**

	3	**5**	**7**	**16**
M−N(1)	2.649(6)	2.615(6)	2.583(7)	2.476(7)
M−N(2)	2.758(6)	2.739(5)	2.715(6)	2.695(6)
M−N(3)	2.629(6)	2.632(6)	2.590(6)	2.483(6)
M−N(4)	2.680(6)	2.594(6)	2.551(7)	2.532(7)
M−O(1)	2.425(5)	2.394(4)	2.368(5)	2.382(6)
M−O(2)	2.381(5)	2.383(5)	2.362(5)	2.245(5)
M−O(3)	2.424(5)	2.348(5)	2.319(5)	2.289(5)
M−O(5)	2.692(5)	2.697(5)	2.698(6)	2.737(6)
M−O(6)	2.641(5)	2.614(5)	2.557(6)	2.413(6)
O(3)−M−O(2)	96.50(17)	95.1(2)	92.44(19)	90.0(2)
O(2)−M−O(1)	78.04(17)	71.5(2)	70.83(19)	75.2(2)
O(2)−M−N(4)	70.06(17)	70.3(4)	71.3(2)	74.3(2)
O(3)−M−O(6)	77.21(18)	115.3(2)	116.39(19)	76.2(2)
O(1)−M−O(6)	147.59(18)	145.8(2)	144.87(19)	141.6(2)
O(3)−M−N(1)	135.99(18)	89.3(2)	89.0(2)	136.5(2)
O(1)−M−N(1)	67.35(17)	68.0(2)	68.49(19)	69.3(2)
O(6)−M−N(1)	137.93(17)	139.1(2)	138.89(19)	137.6(2)
O(2)−M−N(3)	164.12(18)	137.9(2)	136.4(2)	157.2(2)
N(4)−M−N(3)	125.40(18)	126.2(2)	126.9(2)	128.5(2)
N(1)−M−N(3)	95.03(19)	83.6(2)	83.8(2)	90.2(2)
O(2)−M−O(5)	68.76(16)	68.3(2)	67.71(19)	71.8(2)
N(4)−M−O(5)	69.63(18)	112.3(2)	112.1(12)	66.8(2)
O(5)−M−N(2)	112.30(17)	113.1(2)	112.46(19)	111.5(2)
O(3)−M−N(4)	139.07(17)	162.4(2)	160.4(2)	133.2(2)
O(1)−M−N(4)	136.73(17)	88.4(2)	86.9(2)	141.7(2)
O(2)−M−O(6)	114.59(17)	75.7(2)	76.16(19)	120.7(2)
N(4)−M−O(6)	74.39(18)	71.5(2)	71.2(2)	75.1(2)
O(2)−M−N(1)	90.03(18)	137.1(2)	137.9(2)	90.4(2)
N(4)−M−N(1)	83.89(18)	95.0(2)	95.9(2)	88.3(2)
O(3)−M−N(3)	69.53(17)	71.2(2)	72.4(2)	74.1(2)
O(1)−M−N(3)	90.02(18)	137.5(2)	138.9(2)	83.7(2)
O(6)−M−N(3)	70.75(18)	75.2(2)	75.0(2)	72.0(2)
O(3)−M−O(5)	69.48(17)	68.9(2)	69.29(19)	66.4(2)
O(1)−M−O(5)	124.38(17)	123.7(2)	124.36(19)	123.2(2)
O(6)−M−O(5)	47.77(16)	47.9(2)	48.24(18)	49.5(2)
N(3)−M−O(5)	111.10(17)	69.7(2)	68.7(2)	114.5(2)
O(2)−M−N(2)	129.66(18)	132.9(2)	134.16(19)	132.4(2)
N(4)−M−N(2)	64.63(18)	66.2(2)	66.8(2)	65.5(2)
N(1)−M−N(2)	64.99(18)	65.0(2)	65.5(2)	65.0(2)
N(3)−M−N(2)	65.80(18)	64.9(2)	65.5(2)	67.5(2)
N(1)−M−O(5)	150.25(19)	149.6(2)	148.8(2)	152.3(2)
O(3)−M−N(2)	132.28(17)	130.6(2)	131.9(2)	136.2(2)
O(1)−M−N(2)	123.24(17)	123.1(2)	122.98(19)	124.9(2)
O(6)−M−N(2)	73.17(17)	74.3(2)	73.7(2)	72.6(2)
O(3)−M−O(1)	71.59(16)	77.4(2)	77.26(19)	68.7(2)
Y(2)−O(1S)				2.328(11)
Y(2)−O(2S)				2.353(7)
Y(2)−O(3S)				2.353(8)
Y(2)−O(7)				2.456(8)
Y(2)−O(9)				2.451(7)
Y(2)−O(10)				2.417(9)
Y(2)−O(11)				2.403(7)
Y(2)−O(14)				2.430(7)
Y(2)−O(15)				2.380(7)

(20) Drew, M. G. B.; Marrs, D.; Hunter, J.; Nelson, J. *J. Chem. Soc., Dalton Trans.* **1992**, 11.

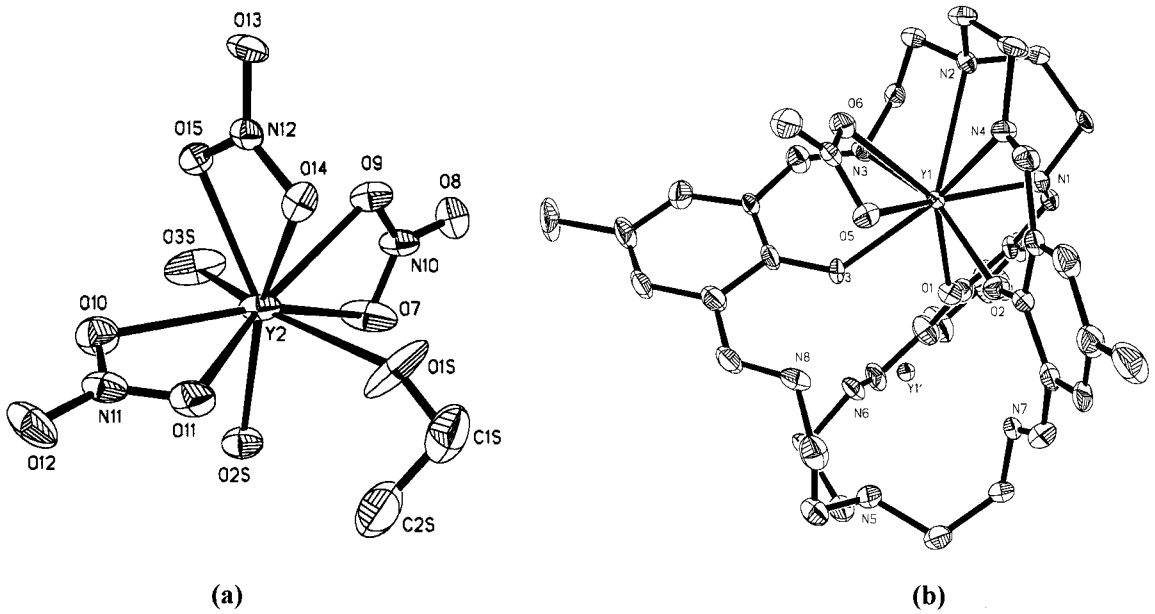

Figure 2. (a) X-ray crystal structure of $[Y(NO_3)_3(H_2O)_2EtOH]$ showing the atomic numbering scheme. Hydrogen atoms have been omitted for simplicity. The ORTEP plot is at the 30% probability level. (b) X-ray crystal structure of the cation $[YL(NO_3)]^{2+}$; The minor position of the yttrium atom is indicated by Y′ but no bonds are attached. Thermal ellipsoids are shown at 30% probability. For clarity, the hydrogen atoms are not included.

two oxygen atoms of a bidentate nitrate ion. N(1), N(3), N(4), and O(6) form a plane (deviation form planarity 0.0714 Å); Y(1) is located 0.9544 Å below it and 1.5496 Å above the plane formed by the three phenoxy oxygen atoms, O(1), O(2), and O(3). Again the coordination geometry around the metal ion can be best described as a distorted monocapped dodecahedron where the O(5) of the coordinated nitrate group is the atom that is capping the dodecahedron. The minor position of the yttrium ion, Y(1)′, is located at the other end of the macrobicycle, where it also forms close contacts with seven donor atoms of the macrobicycle [Y(1)′−N(5), 2.419(13); Y(1)′−N(6), 2.320(14); Y(1)′−N(7), 2.319(13); Y(1)′−N(8), 2.574(14); Y(1)′−O(1), 2.207(13); Y(1)′−O(2), 2.613(13); and Y(1)′−O(3), 2.287(13) Å] and it is placed between the planes formed by O(1), O(2), O(3) and N(6), N(8), N(9), at 1.6732 Å below the first one and at 0.5640 Å above the second one. In this minor position of the yttrium ion there is room enough for a nitrate around the metal ion; nevertheless we could not find it probably due to its electron density is masked by the residual density because of the occupancy of the yttrium ion in this position is only 0.05(1).

The macrobicycle L is twisted around the axis that passes through both bridgehead nitrogen atoms and adopts a *sss* conformation with both nitrogen atoms disposed in *endo* similar to that present in **3**, **5**, and **7**; nevertheless, the helix is found to be clearly more distorted in the case of **16**. Angles between planes defined by phenolic rings have values of 62.6°, 95.3°, and 113.9°; distances between phenoxy oxygen atoms are 2.638, 2.826, and 3.206 Å and between both bridgehead nitrogen atoms 8.32 Å, shorter than those found in cerium, neodymium and europium complexes. These data show how the ligand can expand or contract to fit the metal size into its cavity.

Proton NMR Spectra of the Diamagnetic Complexes. ^1H NMR spectra of the La, Lu and Y complexes were obtained in D_2O solution (see examples in Figure 3a and c) and were assigned on the basis of signal intensities and of COSY and NOESY two-dimensional experiments. These spectra indicate that the systems have an effective C_3 symmetry in solution, with the metal ion not centered in the cavity of the cryptand (see Chart 2 for the outline solution structure of the complexes and the atom numbering used in the NMR study). Geminal CH_2 protons of the ethylenediamino (en) moieties gave strong COSY and NOESY cross-peaks. NOESY (0.5 s mixing time) cross-peaks were also observed between imino/phenolic, imino/en, and methyl/phenolic proton pairs located at distances shorter than 2.6 Å in the X-ray crystal structure of **7**. Although the specific axial/equatorial CH_2 proton assignments were not possible on the basis of the 2D NMR spectra, they were carried out for the metal-bound en moiety (see Figure 3) using the stereochemically dependent proton shift effects, resulting from the polarization of the C−H bonds by the electric field effect caused by the cation charge, as predicted[21] from the X-ray crystal structure of **7**.

While in the La complex (Figure 3a) only four resonances are observed for the CH_2 protons of the two types (metal bound and unbound) of en moieties in aqueous solution, in the Y and Lu complexes (Figure 3b) eight peaks are observed. Indeed, while in the Lu complex these resonances are sharp at 298 K, in the Y complex the signals are considerably broader, and in the La chelate no couplings are observed in the proton spectrum. This is indicative of an increased rigidity of the en moieties in aqueous solution upon decreasing the ionic radius of the metal ion. The eight proton ethylene resonances of the Lu complex gradually broaden above 298 K, reflecting intramolecular conformational exchange processes, which for the five-membered chelate rings formed by the metal-bound en moiety is a $\delta \leftrightarrow \lambda$ conformational interconversion. Under conditions of fast exchange there is an effective C_3 axis of symmetry in the structure of the complex shown in Chart 2. When the temperature is increased to 353 K, coalescence of the peaks due to the H_{2ax} and H_{2eq} protons is observed. A band-shape analysis[21] was carried out on the H_{2ax} resonance over the 298−334 K temperature range in order to calculate the activation parameters for the conformational interconversion process. A plot of k/T vs $1/T$ [$k = (k_bT/h)\exp(\Delta S^{\ddagger}/R - \Delta H^{\ddagger}/RT)$, where k_b is the Boltzmann constant, T is the absolute temperature, k

(21) Harris, R. K. *Nuclear Magnetic Resonance Spectroscopy: A Physicochemical View*; Pitman: London, 1983.

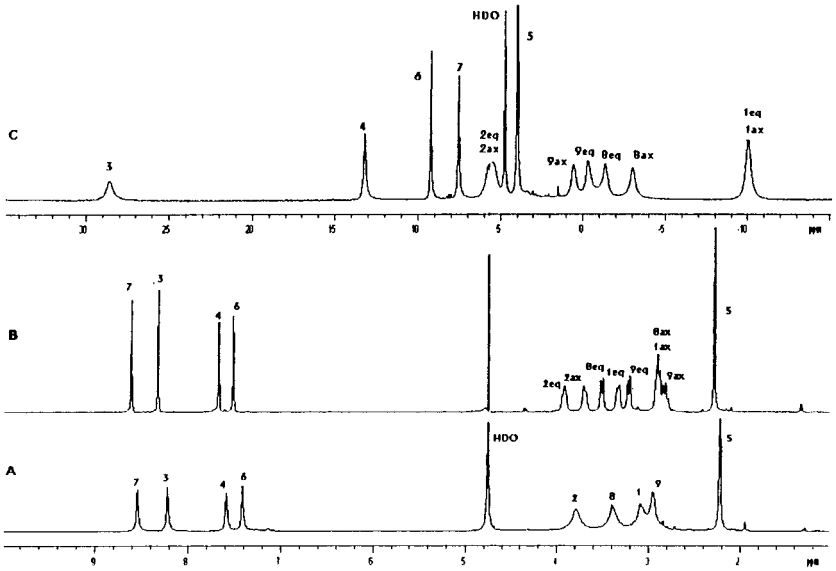

Figure 3. 500 MHz proton NMR spectra of $[Ln(L)]^{3+}$ complexes in D_2O solution (5 mM, pD = 5.8, 25 °C): (a) La^{3+} complex; (b) Lu^{3+} complex; (c) Pr^{3+} complex.

Chart 2

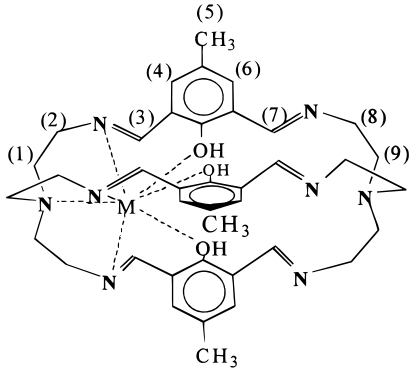

is the rate constant, $\Delta G^{\ddagger}$, $\Delta H^{\ddagger}$, and $\Delta S^{\ddagger}$ are the activation free energy, enthalpy, and entropy, respectively] yields the activation parameters ($\Delta G^{\ddagger}$= 70 + 3 kJ mol^{-1}, $\Delta H^{\ddagger}$ = 76 + 3 kJ mol^{-1}, $\Delta S^{\ddagger}$ = 21 + 1 J K^{-1} mol^{-1}, k = 3.3 ± 0.1 s^{-1} at 298 K). The activation free energy value obtained is of the same order of magnitude as that reported for La(DOTA)$^{-}$ ($\Delta G^{\ddagger}$ = 60.7 kJ mol^{-1} at 300 K).[12b]

Proton NMR Spectra of the Paramagnetic Complexes. ^{1}H NMR spectra of the paramagnetic $[Ln(L)]^{3+}$ complexes (Ln = Ce−Yb except Pm and Gd) were obtained in D_2O solution (see illustration for $[Pr(L)]^{3+}$ in Figure 3c). A summary of the ^{1}H LIS values determined for those $[Ln(L)]^{3+}$ complexes at 298 K is given in Table 3. All the LIS values were measured relative to the La complex for the earlier members of the lanthanide series and relative to the Lu complex for the later members of the series. For the Sm complex, with its very small isotropic shifts and sharp signals, many assignments could be made by simple comparison with the diamagnetic La complex. The ^{1}H NMR spectra of the paramagnetic complexes were assigned by plotting the experimental LIS values according to eqs 2 and 3 (see later), allow for permutations of any two selected nuclei and then determining which particular assignment of peaks gives the best straight lines. For the Ce, Pr, Nd, and Eu complexes assignments were confirmed on the basis of signal integrals, and a comparison of the experimental and calculated (on the basis of the X-ray crystal structure of **7**) relative proton pseudocontact LIS and T_1 LIR values using the LISLIR program, which performs a linear least-squares fitting of the data. This procedure has some circular reasoning, as it assumes that the solution structure is the same as in the solid state, which is what is demonstrated later with the LISLIR calculations. However, in this procedure as well as in other similar ones,[11,22] if a good fit between experimental and calculated data is obtained, both the assignments and the solution structure are acceptable. For the remaining paramagnetic lanthanide complexes, the resonance assignments were made in a similar way but the relative LIR values were obtained from the signal line widths. This procedure could not be completed for all protons due to the extreme line broadening of some of the resonances.

Separation of Contact and Pseudocontact Shift Contributions. The substantial LIS values, induced by the paramagnetic Ln(III) ions in the NMR signals of protons located in the vicinity of the metal center,[23] has two contributions, the Fermi contact (δ_c) and the dipolar or pseudocontact shifts (δ_{pc}),

$$\Delta_{i,j} = \delta_c + \delta_{pc} = A_i\langle S_z\rangle_j + G_i A_2^{\circ}\langle r^2\rangle C_j \qquad (1)$$

where $\Delta_{i,j}$ is the LIS of the observed nucleus i induced by the Ln ion j, A_i is the hyperfine coupling constant of nucleus i, which governs the contact interaction between that nucleus and the Ln ion, $A_2^{\circ}\langle r^2\rangle$ is the crystal field parameter, which is a measure of the strength of interaction between a given lanthanide ion and the ligand donor atoms and G_i is the geometric factor of nucleus i that contains the structural information about the complex inherent in the dipolar shift. $\langle S_z\rangle_j$ and C_j are, respectively, the spin expectation value and the magnetic constant (Bleaney factor) of the paramagnetic lanthanide,[23] which have been tabulated.[24,25] For a complex with effective axial magnetic symmetry,

$$G_i = (3\cos^2\theta - 1)/r^3 \qquad (2)$$

where r is the Ln−nucleus distance and θ is the angle between

(22) Kemple, M. D.; Ray, B. D.; Lipkowitk, K. B.; Prendergast, F. G.; Rao, B. D. N. *J. Am. Chem. Soc.* **1988**, *10*, 8275.
(23) Peters, J. A.; Huskens, J.; Raber, D. J. *Prog. NMR Spectrosc.* **1996**, *28*, 283.
(24) (a) Golding, R. M.; Halton, M. P. *Aust. J. Chem.* **1972**, *25*, 2577. (b) Pinkerton, A. A.; Rossier, M.; Stavros, S. *J. Magn. Reson.* **1985**, *64*, 420.
(25) Bleaney, B. *J. Magn. Reson.* **1972**, *8*, 91.

Table 3. ^{1}H LIS Values (ppm) for the $[Ln(L)]^{3+}$ Complexes[a]

Ln^{3+}	H_{1ax}	H_{1eq}	H_{2ax}	H_{2eq}	H_3	H_4	H_5	H_6	H_7	H_{8ax}	H_{8eq}	H_{9ax}	H_{9eq}
Ce^{3+}	11.52	11.52	−0.39	−0.11	−9.90	−3.70	−1.19	−1.04	0.80	4.62	3.52	2.27	3.06
Pr^{3+}	12.99	13.03	−1.78	−1.69	−20.38	−5.64	−1.79	−1.83	0.98	5.67	4.32	2.82	3.69
Nd^{3+}	2.02	3.18	−1.98	−0.60	−19.21	−3.06	−1.01	−1.56	0.32	2.72	1.98	1.23	1.79
Sm^{3+}	0.30	0.20	0.02	0.01	0.54	−0.86	−0.14	−0.02	0.52	*b*	*b*	*b*	*b*
Eu^{3+}	6.61	3.53	2.40	2.32	30.61	3.91	0.75	2.09	−0.01	0.15	0.20	0.25	0.25
Tb^{3+}	133.51	116.62	38.69	18.21	−28.98	−29.02	−8.98	*b*	*b*	*b*	*b*	*b*	*b*
Dy^{3+}	95.56	85.32	29.00	14.02	−23.06	−23.12	−7.56	*b*	*b*	*b*	*b*	*b*	*b*
Ho^{3+}	40.00	48.30	16.90	7.78	−18.39	−18.23	−4.91	*b*	*b*	*b*	*b*	*b*	*b*
Er^{3+}	−26.94	−32.15	8.79	3.42	26.10	*b*	0.06	*b*	*b*	*b*	*b*	*b*	*b*
Tm^{3+}	−54.53	−31.63	10.67	8.40	33.11	*b*	2.91	*b*	*b*	*b*	*b*	*b*	*b*
Yb^{3+}	−32.07	−11.78	0.60	0.38	12.95	*b*	0.67	*b*	*b*	*b*	*b*	*b*	*b*

[a] Positive values are to lower δ (ppm) values. [b] The resonances could not be assigned.

Table 4. Separation of Pseudocontact and Contact Contributions to the Observed LIS in the $[Ln(L)]^{3+}$ Complexes

	Ce → Eu		Tb → Yb	
nucleus	A_i	$A_2^\circ\langle r^2\rangle G$	A_i	$A_2^\circ\langle r^2\rangle G$
H_{1ax}	1.81± 0.28	−2.05 ± 0.22	0.33 ± 0.32	−1.06 ± 0.09
H_{1eq}	1.30± 0.25	−1.78 ± 0.15	0.42 ±0.34	−0.95 ± 0.11
H_{2ax}	0.55 ± 0.13	−0.06 ± 0.04	0.79 ± 0.13	−0.09 ± 0.05
H_{2eq}	0.40 ± 0.10	−0.01 ± 0.04	0.33± 0.05	−0.05 ± 0.02
H_3	3.48 ± 0.06	1.03 ± 0.05	0.57 ± 0.17	0.52 ± 0.05
H_4	0.25 ± 0.04	0.49 ± 0.04	0.40 ± 0.15	0.55 ± 0.05
H_5	0.01 ± 0.02	0.18 ± 0.01	−0.11 ± 0.01	0.06 ± 0.01
H_6	0.21 ± 0.01	0.13 ± 0.01	*a*	*a*
H_7	0.06 ± 0.01	−0.13 ± 0.01	*a*	*a*
H_{8ax}	0.15 ± 0.06	−0.75 ± 0.05	*a*	*a*
H_{8eq}	0.11 ± 0.06	−0.50 ± 0.07	*a*	*a*
H_{9ax}	0.21 ± 0.06	−0.54 ± 0.06	*a*	*a*
H_{9eq}	0.65 ± 0.06	−0.44± 0.07	*a*	*a*

[a] Not determined.

the Ln−nucleus vector and the main axis of symmmetry of the magnetic susceptibility tensor of the complex. The contact and pseudo-contact contributions can then be separated according to a structure-independent method,[26] which is based on the rearrangement of eq 1 into the linear forms given by eqs 3 and 4:

$$\Delta_{i,j}/C_j = A_i\langle S_z\rangle_j/C_j + G_iA_2^\circ\langle r^2\rangle \quad (3)$$

$$\Delta_{i,j}/\langle S_z\rangle_j = A_i + G_iA_2^\circ\langle r^2\rangle C_j/\langle S_z\rangle_j \quad (4)$$

Thus, for a series of isostructural complexes, plots of $\Delta_{i,j}/C_j$ against $\langle S_z\rangle_j/C_j$ and of $\Delta_{i,j}/\langle S_z\rangle_j$ versus $C_j/\langle S_z\rangle_j$ for equivalent nuclei along the lanthanide series should be linear, with intercepts equal to $G_iA_2^\circ\langle r^2\rangle$ and A_i, respectively. However, deviations from linearity sometimes occur, even when there is not a drastic structural change along the lanthanide series,[12f,23] which might be due to variation of the crystal field parameter $A_2^\circ\langle r^2\rangle$.[27,28]

The pseudocontact and contact contributions to the observed LIS values were separated by using eqs 3 and 4, and the results are reported in Table 4. These show that nearly all protons have contributions from both contact and pseudo-contact sources. The contact contribution is relatively small for most shifts, and is largest for the coordinated imino protons. Then, the observation that the range of pseudo-contact dominated LIS values for Tb is significantly larger than for Dy for all protons (Table 3), quite unexpected from their relative C_j values,[24,25] should reflect variations of the crystal field parameter $A_2^\circ\langle r^2\rangle$. In the cases

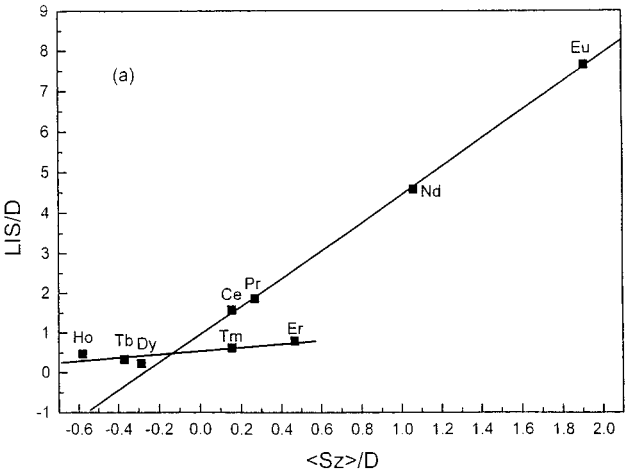

Figure 4. Plot for separation of contact and pseudocontact contributions to the proton LIS data (H_3 protons) according to eq 3.

where the contact shifts are small, the use of eq 3 leads to large errors in the A_i values, and these were obtained from plots based on eq 4. Plots of $\Delta_{i,j}/C_j$ against $\langle S_z\rangle_j/C_j$ and of $\Delta_{i,j}/\langle S_z\rangle_j$ versus $C_j/\langle S_z\rangle_j$ should yield a unique value for A_i and the product $A_2^\circ\langle r^2\rangle G_i$, provided these values are independent of the lanthanide cation and assuming that the complexes are isostructural. However, many of these plots do not follow a single linear correlation but rather divide into two groups (Ln = Ce − Eu and Ln = Tb − Yb) with a "break" coming near the middle of the lanthanide series as illustrated in Figure 4 for the H_3 protons. These same plots for the other nuclei also show "breaks", more evident for some nuclei than for others.

Lanthanide-Induced Relaxation Rates. The lanthanide induced relaxation (LIR) enhancement effects consist of inner-sphere and outer-sphere mechanisms. The latter is usually relative small and, therefore, often neglected.[23] The inner-sphere relaxation rates may have contributions from the contact, dipolar, and Curie mechanisms. The relative importance of the various relaxation mechanisms has been analyzed in detail,[23] and it has been concluded that the contact contributions are small and may be neglected. Also, although the dipolar interaction usually dominates the spin−lattice relaxation of protons, at high magnetic fields the Curie contribution cannot be neglected, even for small complexes of Ln(III) ions (Ln ≠ Gd),[29] in particular in the second half of the series (high μ_{eff}).[30] As both relaxation rate enhancement contributions have the same dependence on the distance r between the nucleus under study and the Ln(III),

(26) Reilley, C. N.; Good, B. W.; Allendoerfer, R. D. *Anal. Chem.* **1976**, *48*, 1446.
(27) Reuben, J. *J. Magn. Reson.* **1982**, *50*, 233.
(28) Ren, J.; Sherry, A. D. *J. Magn. Reson.* **1996**, *111B*, 178.
(29) Bertini, I.; Capozzi, F.; Luchinat, C.; Nicastro, G.; Xia, Z. *J. Phys. Chem.* **1993**, *97*, 6351.
(30) Aime, S.; Barbero, M.; Botta, M.; Ermondi, G. *J. Chem. Soc., Dalton Trans.* **1992**, 225.

Table 5. Comparison of Calculated[a] and Observed[b] Proton Pseudocontact LIS Values for the Paramagnetic $[Ln(L)]^{3+}$ Complexes and of Calculated[a] Lanthanide Induced Relaxation (LIR)[c] Enhancements and Experimental Values for the $[Eu(L)]^{3+}$ Complex

	Ln (Ce → Eu)				Ln (Tb → Yb)		
nucleus	LIS (calc)[a]	$A_2^\circ \langle r^2\rangle G$	R_{1M}(calc)[a]	R_{1M}(exp)[d]	nucleus	LIS (calc)[a]	$A_2^\circ \langle r^2\rangle G$
H_{1ax}	−2.10	−2.05	61.03	59.44	H_{1ax}	−1.04	−1.06
H_{2ax}	−0.09	−0.06	61.72	67.95	H_{1eq}	−0.99	−0.95
H_3	0.89	1.03	24.17	22.84	H_{2ax}	−0.12	−0.09
H_4	0.55	0.49	4.08	4.09	H_{2eq}	−0.01	−0.05
H_5	0.11	0.18	0.59	0.66	H_3	0.48	0.52
H_6	0.00	0.13	1.61	1.16	H_4	0.57	0.55
H_7	−0.29	−0.13	2.92	2.96	H_5	0.07	0.06
H_{8eq}	−0.52	−0.50	3.48	3.79			
H_{9eq}	−0.41	−0.44	1.25	1.27			

[a] Values calculated using the program LISLIR. [b] The observed proton pseudocontact LIS values (LIS(exp)) are taken as the experimentally obtained $A_2^\circ \langle r^2\rangle G$ values of Table 4. [c] The LIR is represented by the symbol R_{1M}. [d] Experimental data for the Eu(III) complex.

their effect can be combined to

$$R_{1M} = 1/T_{1,M} = k/r^6 \qquad (5)$$

where k is a constant. Application of this equation allows the determination of relative r values in the complexes without the need to have good estimates for the correlation times τ_c for the nuclear−electronic dipolar interaction of the complex, needed to calculate absolute r values. These correlation times are T_{1e} (the electronic spin−lattice relaxation time[31]) for the dipolar interaction in Ln(III) (Ln ≠ Gd) complexes or τ_R (the rotational correlation time) for the dipolar interaction in Gd(III) complexes and the Curie spin contribution.[23]

The paramagnetic contributions to the proton spin−lattice relaxation rates, R_{1M}, also called lanthanide-induced relaxation (LIR) effects (see Table 5), were obtained by measuring the R_1 values for the Eu(III) complex and correcting them for the diamagnetic contribution by subtracting the relaxation rates of the same protons observed for the La(III) complex.

Comparison between the Experimental and Calculated LIS and LIR Values. The atomic coordinates from the X-ray crystal structures of the Nd and Y complexes were used to assess the agreement between the experimental proton LIS and LIR values and those calculated using the LISLIR program, for the first and second half of the lanthanide series, respectively. The LISLIR program allows to vary the location of the lanthanide ion and of the main magnetic axis in the cryptand cavity and calculate the best fit between the experimental and calculated LIS (assuming axial symmetry) and LIR data. The calculated LIS and LIR values of pseudo-symmetry-related nuclei were averaged before comparison to experimental values. The best solutions found showed excellent agreement between the crystal and solution structures of the complexes, as expressed in the R factors obtained.[15] The comparison between the experimental and calculated LIS and LIR for the best solutions is reported in Table 5.

For the lighter lanthanides, the best solution gave $R = 0.0984$ and $R = 0.1264$ for the LIS and LIR, respectively, and a total $R = 0.1151$. This solution structure corresponds to a Ln−N(2) distance of 2.44 Å, 0.3 Å shorter than the range of Ln−N(2) distances (2.76−2.72 Å) found in the crystal structures of the Ce(III)−Eu(III) complexes (see Table 2). The main magnetic axis of the complexes passes through the Ln(III) ion and makes an angle of 5° with the Ln−N(2) vector. For the heavier lanthanides, the best solution, with $R = 0.0512$, was obtained only on the basis of the LIS data available, as no LIR data is available. This solution structure corresponds to a Ln−N(2) distance of 2.18 Å, 0.3 Å shorter than the Ln−N(2) distance (2.48 Å) found in the crystal structure of the Y(III) complex (see Table 2). The main magnetic axis of the complexes coincides with the Ln−N(2) vector.

A detailed comparison of the calculated and experimental structural parameters (Ln−H distances r and angles θ of Ln−H to the principal magnetic axis of the complexes, see Supporting Information), shows a good agreement (within 0.2 Å) for all distances, except for H_5 and H_6. Only a slight decrease of r values occurs for the heavier lanthanide complexes. Thus, the structures of the complexes in solution defined from the proton LIS and LIR data agree quite well with the crystal structures of the Nd and Y complexes, and no drastic structural change occurs along the lanthanide series both in the solid state and in solution structures. On the basis of these results, we can conclude that the origin of the discontinuities in the plots of $\Delta_{i,j}/C_j$ *vs* $\langle S_z\rangle_j/C_j$ and of $\Delta_{i,j}/\langle S_z\rangle_j$ vs $C_j/\langle S_z\rangle_j$ is not a drastic structural difference between the light (Ce−Eu) and heavy (Tb−Yb) complexes, but might arise, as suggested previously,[32] from the normal decrease in Ln-donor atom distances as one progresses along the lanthanide series.

To better understand the origin of these "breaks", we used the detailed solid state and solution structural data, as well as all their proton LIS values, available in this study for a complete series of structurally well-defined Ln(III) cryptate complexes. We have investigated the plots of $\Delta_{i,j}/\langle S_z\rangle_j$ versus $\Delta_{k,j}/\langle S_z\rangle_j$ following eq 6:[27,28]

$$\Delta_{i,j}/\langle S_z\rangle_j = (A_i - R_{ik}A_k) + R_{ik}\Delta_{k,j}/\langle S_z\rangle_j \qquad (6)$$

where $R_{ik} = G_i/G_k$ for two given nuclei i and k. For isostructural complexes, these plots are linear and the slope gives the ratio of the G values of nuclei j and k, whereas the intercept gives the value of $(A_i - R_{ik}A_k)$. The advantage of this procedure is that it does not require the assumption of constancy of the ligand field coefficient $A_2^\circ\langle r^2\rangle$ along the Ln(III) series, a condition found before not to apply to the proton LIS data of the second half of the Ln series of the $Ln(DOTP)^{5-}$ complexes.[28] These plots for each pair of protons originate two straight almost parallel lines, one for the light and the other for the heavy lanthanides. Table 6 shows the values of R_{ik} and $(A_i - R_{ik}A_k)$ obtained by fitting the experimental LIS data to eq 6, which are in good agreement with those calculated from the values of $A_2^\circ\langle r^2\rangle G_i$ and A_i in Table 4. These fitted parameters exclude any drastic change in the values of the ratios of the geometric terms, R_{ik}, for the chelate protons along the lanthanide series, although the geometric terms themselves vary (Table 4). The very different $(A_i - R_{ik}A_k)$ values obtained for the two parts of the series reflect a drastic change in the proton hyperfine constants along the lanthanide series, in agreement with Table 4.

A plot of $G_i \cdot A_2^\circ\langle r^2\rangle$ (Tb−Yb) vs $G_i \cdot A_2^\circ\langle r^2\rangle$ (Ce−Eu) gives also a straight line passing through the origin with slope 0.52 ± 0.01. Thus, the $G_i \cdot A_2^\circ\langle r^2\rangle$ values for the first and second halves of the lanthanide series are proportional, and the R_{ik} ratios are constant along the whole series. This means that the "breaks" in the LIS contact/pseudo-contact separation plots, according to eqs 3 and 4, found in the middle of the Ln series, are due to a variation of both the crystal field parameter

(31) Alsaadi, B. M.; Rossotti, F. J. C.; Williams, R. J. P. *J. Chem. Soc., Dalton Trans.* **1980**, 2147.

(32) Peters, J. A. *J. Magn. Reson.* **1986**, *68*, 240.

Table 6. Comparison of Geometric Ratios and Hyperfine Coupling Constants Obtained from Plots of the Proton LIS Data According to Eq 6[a] and from Data of Table 4[b]

		Ln (Ce → Eu)		Ln (Tb → Yb)	
		R_{ik}	$(A_i - R_{ik}A_k)$	R_{ik}	$(A_i - R_{ik}A_k)$
$i = H_5$, $k = H_3$	exp[a]	0.177 ± 0.009	−0.58 ± 0.06	0.122 ± 0.009	−0.16 ± 0.02
	calc[b]	0.175	−0.60	0.115	−0.17
$i = H_1$[c], $k = H_3$	exp[a]	−2.00 ± 0.11	8.71 ± 0.92	−1.73 ± 0.22	1.49 ± 0.40
	calc[b]	−1.86	8.03	−1.93	1.48
$i = H_4$, $k = H_3$	exp[a]	0.53 ± 0.02	−1.64 ± 0.12	1.03 ± 0.08	0.03 ± 0.03
	calc[b]	0.48	−1.42	1.06	−0.03
$i = H_5$, $k = H_1$[c]	exp[a]	−0.088 ± 0.002	1.19 ± 0.01	−0.068 ± 0.008	−0.06 ± 0.03
	calc[b]	−0.094	0.156	−0.060	−0.09

[a] Parameters obtained from plots of the proton LIS data according to eq 6. [b] Parameters obtained from data of Table 4. [c] The average values of the LIS for H_{1ax} and H_{1eq} were used.

$A_2°\langle r^2\rangle$ and the hyperfine constants A_i. This crystal field parameter has been shown before not to be constant along the second half of the Ln series of the $Ln(DOTP)^{5-}$ complexes, with large variations around Tm.[28]

Table 2 clearly shows that the X-ray experimental Ln−donor distances for the Ce, Nd, Eu, Dy, and Y complexes progressively decrease along the Ln series in the solid state (0.08, 0.15, and 0.1 Å for the amino, imino and phenoxy donor atoms, respectively, from the Ce to the Y complex). On this basis, we propose that this gradual contraction of the Ln coordination polyhedron in solution causes the large variations in $A_2°\langle r^2\rangle$ and in A_i in the middle of the Ln series, but affects the G_i values much less and not at all their R_{ik} ratios.

Conclusions

The whole series of lanthanide cryptate complexes of the Schiff base axial macrobicyclic ligand L of general formula $[LnL][NO_3]_3 \cdot xH_2O$ (Ln = La−Lu,Y) (structure of L is shown in Scheme 1) adopts very similar structures in the solid state, with the nine coordinated metal ion bound asymmetrically in the ligand cavity, and also to two oxygen atoms of a bidentate nitrate anion. As the cation radius decreases, the macrobicycle contracts its cavity, although all complexes adopt the same pseudo-triple-helix conformation around the metal ion, which is clearly more distorted in case of the yttrium complex

In aqueous solution, the proton NMR spectra of the entire series of complexes indicate that they have an effective C_3 symmetry, with the metal ion bound not centered in the cryptand cavity. The conformational rigidity of the five-membered chelate rings formed by the metal-bound ethylenediamino moieties of the bound cryptand, increases upon lanthanide contraction. The proton LIS and LIR effects observed in the paramagnetic complexes allows a quantitative determination of their solution structures, which show excellent agreement with the X-ray crystal structure coordinates of the Nd and Y complexes. Despite the presence of clear "breaks" in the contact/pseudo-contact shift separation plots of the proton LIS values near the middle of the lanthanide series, none of the calculated structural parameters shows important differences between the light and heavy elements of the lanthanide series. Only a slight decrease of the metal−proton distances was found for the later complexes.

We used the detailed solid state and solution structural data, as well as all their proton LIS values, available in this study for a complete series of structurally well-defined Ln(III) cryptate complexes, to fully rationalize the origin of those separation plot "breaks". In the present case, they do not result from a drastic structural difference between the light (Ce−Eu) and heavy (Tb−Yb) complexes, but rather from small changes in the geometry of the complexes along the Ln series due to the decrease of the size of the Ln(III) ion, as suggested previously.[23,32] This gradual contraction and distortion of the coordination polyhedron along the lanthanide series causes a sharp variation of the crystal field parameter $A_2°\langle r^2\rangle$ and the hyperfine constants A_i in the middle of the series, leading to the appearance of "breaks" in the separation plots. However, the dipolar geometric terms of the cryptate protons and their ratios are not affected. The significance of this is that, despite these plot "breaks", the dipolar geometric ratios for the nuclei obtained from them can be safely used in conformational and structural studies in solution.

Acknowledgment. We thank Xunta de Galicia (XUGA 20903B96) and Universidade da Coruña for financial support. C.F.G.C.G. thanks F.C.T., Portugal (Grant Praxis 2/2.1/SAU/1194/95), and BIOMED II (MACE Project) for financial support, COST D8, Program CIENCIA (Portugal) for purchase of the Varian U500 NMR spectrometer, and Dr. J. A. Peters for useful discussions.

Supporting Information Available: X-ray crystallographic files, in CIF format, for **3**, **5**, **7**, and **16** and Figures 1S−6S, showing an ORTEP view of the X-ray crystal structure of the cations $[LnL(NO_3)]^{2+}$ (Ln = Ce, Nd, Eu); structure of the cations $[LnL(NO_3)]^{2+}$ looking down the N(bridgehead)···N(bridgehead) axis (Ln = Ce, Nd, Eu); X-ray crystal structure of the cation $[YL(NO_3)]^{2+}$, view through the N(bridgehead)···N(bridgehead) axis; plot for separation of contact and pseudocontact contributions to the proton LIS data (H_3 protons) according to eq 4; plot of the proton LIS values (H_3 and H_1) according to eq 6; plot of the calculated $G_i \cdot A_2°\langle r^2\rangle$ values (Ln = Tb−Yb) versus $G_i \cdot A_2°\langle r^2\rangle$ (Ln = Ce − Eu) for the H_1, H_2, H_3, and H_5 protons of the paramagnetic complexes of L); and Tables 1S and 2S, listing ^1H shifts for the diamagnetic complexes in D_2O solution and calculated and experimental Ln−proton distances and angles for the $[Ln(L)]^{3+}$ complexes of the first and second half of the lanthanide series). This material is available free of charge via the Internet at http://pubs.acs.org.

IC981314E